J. Bas. Environ. Sci.., 12.4.2 (2025)201-226

Journal of Basic and Environmental Sciences
(J. Bas. Environ. Sci.)
P-ISSN: 2536-9202. e-ISSN: 2356-6388
https://jbes.journals.ekb.eg/

Exploring Monoethylene Glycol-Based Magnetic Carbon Quantum Dots for Enhanced Rheology and Lubricity in Geothermal Drilling Operations

Anwaar O.Ali [1] *, Amany A. Aboulrous[1], Mahmoud F. Mubarak[2], M. I. Abdou[1], A.M. Fadl[1], Wagdy I.El-Dougdoug[3], and Aly A. Aly [3]

[1] Production Department, Egyptian Petroleum Research Institute (EPRI), Nasr City, Cairo, Egypt.

[2] Petroleum Application Department, Egyptian Petroleum Research Institute (EPRI), Nasr City, Cairo, Egypt

[3] Faculty of Science, Benha University, Benha, Egypt.

*** E-mail** : anwaarali.721@gmail.com

ARTICLE INFO

Article History
Received:4/7/2025
Accepted:16/9/2025
Available:20/9/2025

***Keywords*:**
Monoethylene glycol magnetic carbon quantum dots(MEG MCQDs), Geothermal drilling fluids, Rheological properties, Torque reduction, Friction coefficient.

ABSTRACT

This study investigates the incorporation of monoethylene glycol-based magnetic carbon quantum dots (MEG-MCQDs) into geothermal drilling fluids to enhance their rheological properties, torque reduction, and frictional performance under high-pressure, high-temperature (HPHT) conditions. Various concentrations of MEG-MCQDs, ranging from 0.01% to 0.1%, were added to water based mud (WBM) to assess their impact on drilling fluid behavior. The MEG-MCQDs were thoroughly characterized using IR, BET analysis, Zeta potential, DLS, SEM, and TGA to confirm their stability, size, surface characteristics, and thermal properties. The results demonstrated that the key rheological properties, including plastic viscosity and yield point, remained stable, which is essential for maintaining wellbore stability. The torque reduction was notably enhanced, with values reaching up to 52.4% at the highest concentration (0.1%), compared to the blank mud. Additionally, the friction coefficient decreased across all concentrations, with the highest reduction observed at 0.1% MEG-MCQD, showing a clear correlation between nanomaterial concentration and improved lubricity. The MEG-MCQDs nanocomposite also showed excellent thermal stability at 170°C, drastically reducing friction and torque as well as improving fluid loss control and overall drilling efficiency. Such findings open the door to the utilization of MEG-MCQDs for making geothermal drilling more efficient and sustainable.

INTRODUCTION

Geothermal energy is an environmentally friendly renewable resource that is derived from the heat within the Earth (**Igwe, 2021; Akhigbe, 2025**). It is a major capacity for power generation and for heating and cooling purposes as well as being the main protagonist in the world's green energy transition **(Chenic *et al.*, 2022; Eze *et al.*, 2025; Raza *et al.*, 2025**). One of the major factors to ensure the maximum utilization of geothermal energy is the management of geothermal drilling operations. The latter is the performance of drilling fluids during these operations that directly affects the drilling efficiency, the wellbore stability and the lifespan of the equipment (**Jiang *et al.*, 2022; Ghasemi *et al.*, 2025**).

Geothermal drilling fluids are sophisticated chemical formulations designed to serve multiple vital functions: they remove drill cuttings from the wellbore, provide cooling and lubrication to the drill bit, and exert hydrostatic pressure to maintain borehole stability (**Capuano Jr, 2025**). Among different types of drilling fluids, water-based muds (WBMs) are the most extensively used due to their cost-effectiveness, environmental compatibility, and ease of disposal, contrasting with oil- or synthetic-based muds that pose greater environmental and safety (**Ikram *et al.*, 2021;Fan *et al.*, 2025**).

However, the demanding geothermal well conditions characterized by high temperatures, high pressures, and chemically aggressive environments challenge the stability and functional performance of traditional water-based fluids **(Al Jaberi *et al.*, 2025**). A key operational issue involves the formation and control of the filter cake deposited on the wellbore wall during drilling **(Almubarak *et al.*, 2021; Morales, 2025**). A well-formed, thin, and impermeable filter cake is essential to minimize fluid invasion into the formation, which otherwise can result in formation damage, stuck pipe incidents, torque and drag increases, and circulation loss **(Al Shenabrah, 2021; Mashkoor *et al.*,2025).**

To enhance the performance of water-based muds in filtration, rheology, and lubricity under severe geothermal conditions, different natural polymers such as xanthan gum have been utilized (**Ali *et al.*, 2022; Jaya, 2025**). These substances complement the mud by providing the rheological control, minimizing fluid loss, and increasing the viscosity; however, they are usually subjected to critical degradation in the high temperature and pressure (HPHT) atmosphere, which results in the loss of their functions and wellbore stability supply being at risk. As an illustration, traditional WBMs are subjected to fluid loss that is increased by 30–50% and a decrease in plastic viscosity by up to 40% after they have been exposed to 150°C conditions. The identified performance gaps result in insufficient wellbore stability, heightened filtrate invasion, and an elevated risk of operational failures in geothermal drilling. Consequently, geothermal drilling fluids necessitate an additive with elevated thermal stability (**Ahmed *et al.*, 2021; Kalhor Mohammadi *et al.*, 2023**).

In an attempt to find a way over these problems, modern research has looked into using nanotechnology in the fluids for geothermal drilling **(Martin *et al.*, 2023; Meng *et al.*, 2025**). NPs, that are of the size between 1 to 100 nm, provide an increased surface area and peculiar physical and chemical properties that can remarkably lift up the characteristics of the drilling fluids **(Srivastava *et al.*, 2021;Fan *et al.*, 2025**). The main results that have been achieved are: the betterments of rheology, lubricity, filtration control, and thermal stability, the introduction of nanoparticles into drilling fluids is the main reason for it (**Shah *et al.*, 2025**).

Among the various nanomaterials, carbon quantum dots (CQDs) have been the frontrunners because of their nanoscale size, high surface reactivity, biocompatibility

and tunable surface chemistry. The addition of magnetic properties to CQDs also makes it possible for external manipulation and increased sensitivity, which in turn helps to change the properties of the fluid more easily under the influence of dynamic conditions down the hole (**Du *et al.*, 2022; Elugoke *et al.*, 2024**). Monoethylene glycol (MEG), which is most generally known for its high thermal stability, low toxicity, and good compatibility with aqueous systems, is a highly potential base fluid for the dispersion of CQD in geothermal drilling fluids (**Atta *et al.*, 2025**).

The innovative combination of magnetic CQDs based on monoethylene glycol in geothermal drilling applications is designed to tap into synergistic improvements, like efficient rheological control and better lubricity which are essential for successful drilling operations under HPHT conditions(**Medina *et al.*, 2024**). The magnetic CQDs' nanoscale dimensions not only facilitate the even distribution of the fluid but also create strong interfacial interactions with the polymers and the rock surfaces thus, stabilizing the fluid matrix and lowering the friction at the interfaces between the drill string and the borehole (**Cao *et al.*, 2023; Medina *et al.*, 2024; Zhou *et al.*, 2025**).

Recent experiments have validated that MEG-based magnetic CQDs retain their physical structure and functional features after being subjected to hot rolling at 150°C simulating geothermal downhole conditions. They also lead to lower plastic viscosity and better yield stress that, in turn, improve pumpability and the suspension of cuttings while using less energy (**Bardhan *et al.*, 2024; Bassetti *et al.*, 2024**). Besides, their lubricating property is one of the causes of the drop in torque and drag that results in less wear of the equipment and, hence, the decrease of operational risks(**Yang *et al.*, 2023; Duran, 2024**).

This research investigates the production, observation, and performance testing of monoethylene glycol-based magnetic carbon quantum dots for boosting the essential features of geothermal drilling fluids. The discussion focuses on how the nanoadditives assist in enhancing the flow behavior and lubrication properties, their influence on filter cake characteristics and fluid loss management, and their condition in HPHT environments. Furthermore, the conformity of these nanohybrids with traditional water-based mud mixtures guarantees not only the implementation of the process but also the easy change from laboratory to field operations.

This work is an innovative attempt to reinvent the properties of rheology and lubrication of geothermal drilling fluids with a novel MEG-based magnetic CQD system that aims to push the limits of high performance, thermally stable drilling fluids. Such upgrades are fundamental for guaranteeing the performance and environmentally sustainable extraction of geothermal energy, decreasing downtime in operations, and broadening the market potential of geothermal energy projects worldwide.

MATERIAL AND METHODS

1.Material:

In this work, all chemicals and reagents employed in the synthesis of the proposed structure were of analytical grade, ensuring purity levels surpassing 99%. These compounds were employed as received, without further purification. Ferrous sulfate [$FeSO_4.7H_2O$] and ferric nitrate [$Fe(NO_3)_3.9H_2O$] were obtained from Sigma Aldrich Chemical Reagent Co. (USA) and utilized as precursors for the synthesis of Fe_3O_4. A 33% ammonium hydroxide solution (Merck - Germany) was utilized as a precipitating agent in the manufacture of metal oxide. A 30% solution of hydrogen peroxide (H_2O_2) was procured from El-Nasr Company and employed as an oxidizing agent to expedite the hydrothermal reaction during carbonization. Discarded textile industry spools from China. Monoethylene glycol was purchased from Sigma-Aldrich Chemical Reagent Co. (USA). Caustic soda and sodium chloride were obtained from

Sigma-Aldrich Chemical Reagent Company (USA). All studies utilized deionized water procured through a laboratory distillation apparatus.

2.Synthesis of Carbon precursor from Waste Polypropylene

Initially, untreated Waste Polypropylene (waste-PP) was employed as a precursor for carbon production. Waste PP was specifically chosen due to its cost-effectiveness, abundance, and the opportunity for waste valorization, transforming an environmental pollutant into a useful nanomaterial precursor. The waste PP spools were first washed with distilled water to remove surface contaminants such as dirt, oils, and adhesives. After washing, the material was dried in an oven at 60°C for 12 hours to eliminate any residual moisture. Once dried, PP spools undergo a process where they are initially cut into smaller segments, followed by grinding into fine granules using a mechanical grinder for duration of 30 minutes. 5 grams of PP granules were placed in a furnace and subjected to pyrolysis in air at 600°C for duration of 2 hours, leading to the generation of a white precipitate (C-PP), as shown in (**Fig. 1a)**.

3.Synthesis of Carbon Quantum dots (CQDs)

Carbon quantum dots were synthesized using a hydrothermal approach. 3 grams of white precipitate were placed into a 500 ml Teflon-lined stainless steel autoclave containing 180 ml of H_2O_2. After hydrothermal treatment at 180 °C for 12 hours, a gray dispersion of carbon quantum dots (CQDs) was produced. The dispersion of CQDs was subjected to centrifugation at 12.000 rpm for 20 minutes to eliminate residual material. Subsequent to freeze drying, CQDs powder was ultimately obtained, as shown in (**Fig. 1a)**.

4.Synthesis of magnetic Carbon quantum dots (MCQDs)

A composite of MCQDs comprising 10% by weight of ferrous ferric oxide was produced via the chemical co-precipitation technique. A precise quantity of [$Fe(NO_3)_3.9H_2O$] was dissolved in distilled water to formulate a 0.1 M solution. Concurrently, a 0.1 M solution of [$FeSO_4.7H_2O$], holding the requisite quantity to attain the necessary 10% weight percentage in the composite, was synthesized, while a designated CQDs was dissolved in distilled water separately. The three solutions were subsequently amalgamated under vigorous agitation (600 rpm) at ambient temperature for 30 minutes. NH_4OH was subsequently added dropwise to the mixture until a pH of 11 was achieved. After the introduction of ammonia, the reaction vessel was agitated for 30 minutes to guarantee the thorough synthesis of the composite consisting of CQDs and metal-hydroxide. The resulting composite was permitted to precipitate, subsequently collected through filtration, cleaned, and dried in an electric oven for 12 hours at 100 °C. The dehydrated CQDs metal-hydroxide composite was further calcined at 850 °C for 4 hours to yield the equivalent MCQDs composite, as shown in (**Fig. 1a)**.

5.Synthesis of Monoethylene glycol magnetic Carbon quantum dots (MEG-MCQDs)

A quantity of 1 gm of magnetic carbon quantum dots (MCQDs) was gradually introduced into 4 ml of monoethylene glycol (MEG). The mixture was stirred continuously at 500 rpm and maintained at 60°C for one hour to facilitate thorough dispersion. Subsequently, the suspension was subjected to ultrasonic treatment for 30 minutes at the same temperature to disrupt any nanoparticle aggregates and achieve a stable colloidal dispersion, as shown in **Fig. 1a and b**.

6.Preparation of Water-Based Drilling Fluids Containing MEG-MCQDs Nanocomposite

The water-based geothermal drilling fluid system comprises a range of chemical additives, as outlined in Table 1.Water-based drilling fluids were prepared in

laboratory barrels, each corresponding to approximately 350 mL of aqueous base mud. A Hamilton Beach mixer operating at a high speed of 24.000 rpm was used to ensure thorough mixing and uniform dispersion of all ingredients throughout the preparation process.

The preparation followed a controlled mixing sequence: fresh water (251.48 mL) was first poured into the mixing vessel. Sodium chloride (NaCl, 107.77 g) was added gradually with continuous stirring until fully dissolved to adjust the fluid's salinity. Commercial xanthan gum (1.1 g) was slowly introduced to prevent lumping and mixed for 15 minutes to ensure complete hydration and viscosity development. Next, commercial starch (7 g) was added as a fluid loss control agent and mixed for an additional 10 minutes. The fluid's pH was then adjusted by adding 1 g of caustic soda under constant mixing. Calcium carbonate ($CaCO_3$, 12 g) was added as a weighting agent and dispersed evenly by stirring thoroughly. the MEG-MCQDs Nanocomposite additive, serving as a lubricant and thermal stabilizer, was incorporated at varying concentrations (0, 0.01, 0.05, 0.1, 0.25 and 0.5 wt%) relative to the total fluid weight.

Table 1. Water-Based Drilling Fluids Formula

Component	Function	Quantity	Unit
Fresh water	Fluid Base	251.48	Ml
NaCl	Salinity Control	107.77	gm
XC (commercial)	Viscosifier	1.1	gm
Starch (commercial)	Fluid Loss Control	7	gm
Caustic Soda	pH Control	1	gm
CaCO3	Weighting Agent	12	gm
MEG-MCQDs Nanocomposite	Lubricant/Thermal Stabilizer	0, 0.01, 0.03. 0.05, 0.07, and 0.1	wt%

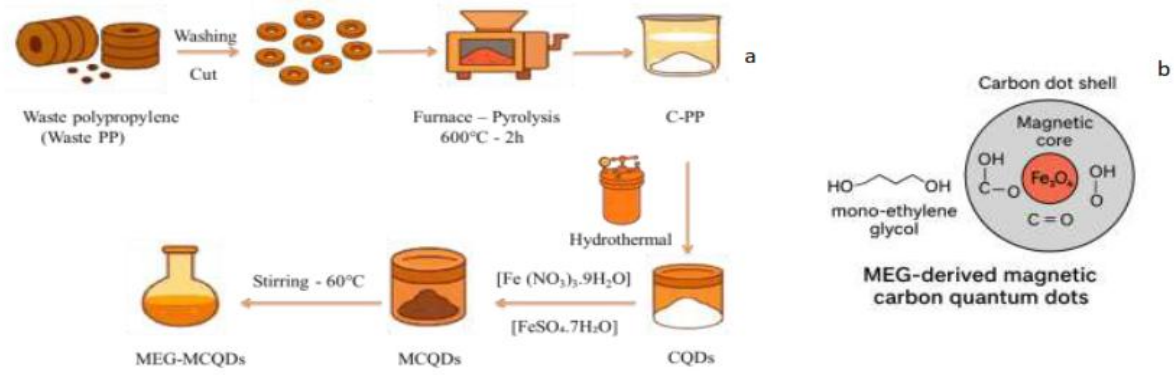

Fig.1. a) Preparation of MEG-Functionalized Magnetic Carbon Quantum Dots (MEG-MCQDs) from Waste Polypropylene, b) Structure of MEG-MCQDs Nanocomposite

7. Drilling Fluids Properties Characteristics

Rheological and Filtration Experiments

The performance of the NC's thermal stability and aging effect was evaluated through tests conducted before hot rolling (BHR) and after hot rolling (AHR). The mud samples underwent rolling in a FANN rolling oven at a temperature of 170 °C. All testing procedures for mud samples and equipment adhered to the standards set by the American Petroleum Institute (API). The filtration volume characteristics of the mud samples were obtained using a standard OFITE LPLT filter press, applying a pressure of 100 psi at atmospheric temperature. The rheological behavior of the mud

samples was examined using an OFITE model 800 viscometer at six distinct speeds (600, 300, 200, 100, 6, and 3 rpm). The analyses yielded rheological parameters, including shear rate, plastic viscosity (PV), and yield point (YP) of the drilling fluid system, derived from the following equations (Ahmed et al., 2024; Bardhan et al., 2024).

Shear rate = $\theta \times 1.7034$ (s^{-1}) (1)

PV = θ_{600}- θ_{300} (mPa.s) (2)

YP = $0.511 \times (\theta 3_{00}$-PV) (Pa) (3)

Where θ is the dial reading at specific speeds (rpm).

Lubricity Test

The lubricity of the mud samples post hot-rolling was assessed utilizing an OFITE EP (Extreme Pressure) and Lubricity Tester. This test was intended to replicate the interaction between the drill string and the wellbore. The measurements and computations were executed in accordance with the procedures and methodologies outlined in the OFITE Lubricity Tester manual. The correction factor (CF), lubricity coefficient (LC), and torque reduction percentage were computed using Equations (4) to (6), respectively (Khandaker *et al.*, 2023).

$$CF = \frac{34}{\text{Water reading}} \quad (4)$$

$$LC = \frac{\text{Mud Reading} \times CF}{100} \quad (5)$$

$$\% \text{ Torque Reduction} = \frac{AL - BL}{AL} \times 100 \quad (6)$$

In equation (4), the value 34 represents the numerical measurement obtained from the torque meter in for deionized (DI) water. The mud reading denotes the torque measurement associated with the base mud and sample muds utilized in the lubricity assessment. Additionally, AL and BL represent the torque measurements for the blank mud and the sample mud, respectively.

8. Characterizations of the prepared Structures

X-ray powder diffraction (XRD) analysis was performed utilizing an X'Pert PRO PANalytical apparatus with a Ni filter (λ=0.15406 nm) to ascertain the structural characteristics of the synthesized materials. The surface characteristics of the structures were assessed utilizing a Quantachrome NOVA 2000. The functional groups of the synthesized composite were analyzed using a Fourier-transform infrared (FTIR) spectrophotometer (Nicolet Is-10, USA). The zeta potential of the nanocomposite was measured using a Zetasizer Nano ZS (Malvern). The molecular vibrations of these samples were analyzed using a LabRAM HR Evolution Raman spectrometer (Horiba, France). Thermogravimetric analysis (TGA) was conducted using the simultaneous TGA model SDTQ 600, USA, under a nitrogen atmosphere, with a heating rate of 10 °C min^{-1} from room temperature to 800 °C. The inner and close morphology was examined using a JEOL JEM-2100 high-resolution transmission electron microscope (HR-TEM). The samples were analyzed using a Quanta-250 FEG scanning electron microscope (SEM) manufactured by FEI, Netherlands. The samples were imaged using a voltage of 20.00 kV and a working distance of 11.7 mm. Scanning electron microscopy (SEM) images were obtained at a magnification of 120,000×, utilizing an Everhart-Thornley detector (ETD) for imaging purposes. The images were captured with a field width of 3.45 μm and a spot size of 3.5 to acquire detailed surface morphology data.

RESULTS AND DISCUSSION

1.Fe_3O_4, CQDS, MCQDs and MEG-MCQDS Characterization

Fig.2a presents the XRD patterns for the composites of Fe_3O_4, CQDS, MCQDs. Peaks observed at approximately 21.9°, 30.3°, 37.1°, and 53.5° correspond to the (111),

(311), (222), and (400) planes of Fe_3O_4 (JCPDS no: 00-004-0429)**(Sani *et al.*, 2021; Zhang *et al.*, 2021**). Furthermore, the detected peaks at 28.39°, 31.53°, 40.59°, and 45.24° correspond to the graphitic carbon Miller indices (0 0 2), (1 1 0), (1 0 0), and (1 0 1) (JCPDS no: 00-001-0640), thereby affirming the polycrystalline nature of the material(**Yalshetti *et al.*, 2024**). The XRD patterns of MCQDs exhibit remarkable changes compared to CQDs and Fe_3O_4, indicating structural modifications. Distinct Fe_3O_4 peaks, such as the (311) reflection at 30.3°, show small shifts or broadening due to lattice strain and interactions with CQDs. The graphitic (002) peak (28.39°) of CQDs might be of lower intensity or shift slightly due to the addition of Fe_3O_4. In addition, peak intensity variations and broadening are present, which suggest that there is some change in the crystallinity and particle size of the material(**Holder & Schaak, 2019**). The observed differences evidence the presence of the Fe_3O_4 and CQDs parts in the resulting composite which are of changed crystallographic properties. The lattice crystal sizes of the synthesized samples were estimated using the Scherrer equation, giving approximate values of ~12.9 nm for Fe_3O_4, ~7.6 nm for CQDs, and ~11.1 nm for MCQDs.

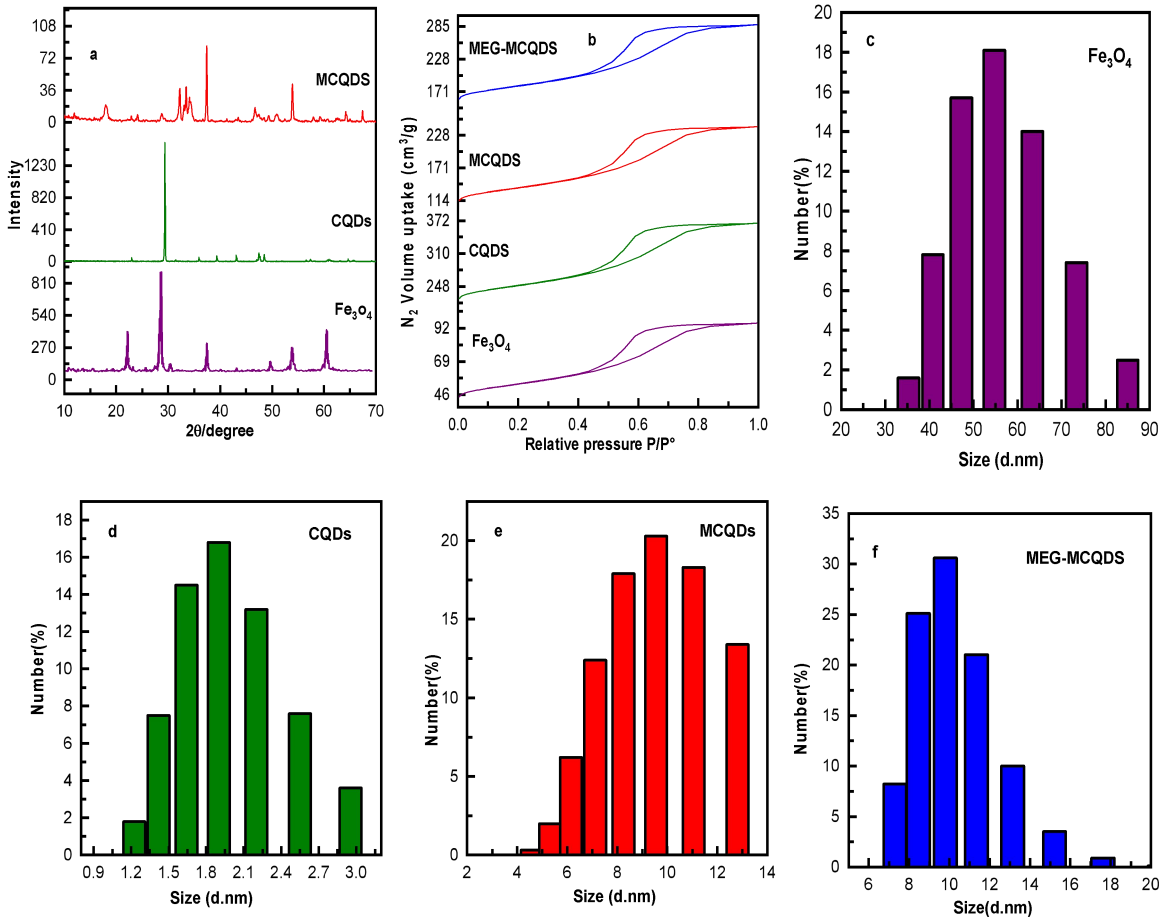

Fig.2. (a) XRD, (b) N_2 adsorption-desorption isotherms, (c),(d), (e) and (f) CQDS, MCQDs, and MEG-MCQDs composites, respectively.

The surface area of Fe_3O_4, CQDS, MCQDs and MEG-MCQDS materials are shown in **Fig. 2b**, and the quantitative results are given in **Table 2**. The magnetic material Fe_3O_4 has the lowest surface area (90 m^2/g) and pore volume (0.12 cc/g) among the materials, but the biggest average pore diameter (5.2 nm) that corresponds to a more compact structure characterized by relatively large pores. On the other hand,

CQDS has the highest surface area (360 m^2/g) together with the small pore sizes (2.7 nm), which are the high disperse and nanostructured nature that facilitates the extensive surface exposure. The MCQDS and MEG-MCQDS composites respectively exhibit intermediate properties with surface areas of 245 and 280 m^2/g and pore volumes of 0.5 and 0.35 cc/g. These properties indicate that these composites are ideal to carry out the properties of Fe_3O_4 and CQDS synergistically, thus enabling a tunable balance of surface area and porosity suitable for accessing and utilizing the functional performance of surface.

These results suggest that the composites combine the advantages of Fe_3O_4 and CQDs, offering a tunable balance of surface area and porosity. In the context of WBM formulations, higher surface area facilitates better interaction with fluid additives, contributing to stable dispersion of the nanocomposite. Meanwhile, appropriate pore structure supports improved fluid loss control and enhances lubricity by reducing solid–solid contact at high temperatures. Thus, the BET data provide direct evidence of how MEG-MCQDs can maintain rheological stability and improve overall WBM performance under geothermal drilling conditions.

Figure 2c, d, e, and **f** show the particle size distribution investigation of Fe_3O_4, CQDs, and their combination materials. The Fe_3O_4 nanoparticles reveal a size of less than 55 nm on average. On the one hand, the CQDs are of a very tiny size, about 1.9 nm, which is entirely in line with the nature of quantum dots. After the union of CQDs and Fe_3O_4, the MCQDs composite of the latter shows the intermediate average size of 9.5 nm, thus proving that the two substances were effectively modified and their interaction was very strong. Moreover, the DLS analysis of the MEG-MCQDs composite is indicative of an average particle size of 9.8 nm, which is consistent with the steady formation of the modified composite structure. The zeta potential measurements of Fe_3O_4, CQDS, MCQDs and MEG-MCQDS composites (**Fig. 3a**) demonstrate the differences in surface charge of the samples that were investigated. The data for pure Fe_3O_4 show a positive zeta potential of 20 mV, indicating moderate colloidal stability due to electrostatic repulsion between particles. The surface of CQDs is negatively charged, as they have a zeta potential of -20.7 mV, which can be attributed to oxygen-containing functional groups present on their surface. The MCQDs have a zeta potential of 7.5 mV, providing evidence of the effective combination of Fe_3O_4 and CQDs, which alters the surface charge while maintaining dispersion stability. The MEG-MCQDs exhibit a zeta potential of 17.9 mV, surpassing that of MCQDs. This enhancement reflects improved surface charge modification and greater dispersion stability as a result of surface functionalization.

Thermogravimetric analysis (TGA) was performed to evaluate the thermal stability and compositional characteristics of Fe_3O_4 nanoparticles as shown in Fig.3b, CQDs, MCQDs, and functionalized MEG-MCQDs. Fe_3O_4 exhibited minimal weight loss (~4.2%) below 150 °C, which is attributed to surface-adsorbed moisture, and demonstrated excellent thermal stability with negligible degradation, retaining ~95.8% residual mass up to 800 °C, confirming the robustness of its inorganic magnetic core. In contrast, CQDs showed a single-stage weight loss pattern rather than two stages: negligible moisture evaporation (<1%) was observed below 150 °C, followed by a sharp mass loss of ~44% occurring between 600–750 °C due to decomposition of their carbonaceous core and surface functional groups, leaving ~56% residual mass at 800 °C, indicating moderate thermal stability inherent to organic nanomaterials.

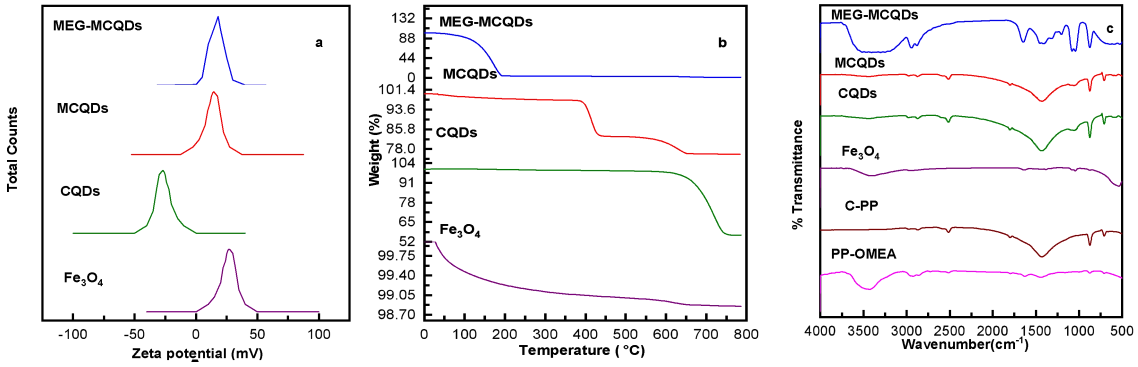

Fig.3. (a) Zeta potential , (b)TGA of Fe_3O_4, CQDS, MCQDs and MEG-MCQDs composites and (c) FTIR of PP waste, C-PP, Fe_3O_4, CQDS, MCQDs and MEG-MCQDs composites.

The TGA profile of MCQDs revealed a composite thermal behavior, reflecting contributions from both Fe_3O_4 and CQDs. An initial mass loss of ~3.5% below 150 °C corresponded to moisture removal, while the carbonaceous components underwent a sharp decomposition of ~13% between 350–450 °C, followed by an additional ~8% weight loss between 500–650 °C, leaving ~75.5% residual mass at 800 °C. This substantial inorganic residue from Fe_3O_4 indicated successful integration of magnetic nanoparticles with carbon dots. An initial ~12% loss below 150 °C was due to moisture and volatile species, followed by a sharp decomposition of ~78% between 150–350 °C, mainly attributable to the degradation of MEG surface groups and the CQD matrix. A minor additional weight loss of ~3% occurred between 400–650 °C. The sample retained only ~7% residual mass at 800 °C, which is significantly lower than MCQDs, reflecting the dominance of organic functionalization but still confirming the presence of the Fe_3O_4 core as the stable inorganic residue.

Although MEG functionalization lowers thermal stability relative to MCQDs, the decomposition onset (~150 °C) remains above the operational threshold for medium-enthalpy geothermal drilling fluids (typically ≤200 °C). This confirms that MEG-MCQDs are thermally stable within the target application window, while also offering improved dispersion stability, lubricity, and interaction with fluid additives essential for maintaining rheological performance under geothermal drilling conditions.

Fig.3c illustrates the IR of Fe_3O_4, CQDS, MCQDs and MEG-MCQDs composites. The infrared spectrum of waste polypropylene displays distinct peaks corresponding to the different vibrational modes of its molecular structure. A broad band near 3450 cm^{-1} is not intrinsic to pure polypropylene but is attributed to hydroxyl (-OH) groups formed during environmental degradation processes such as UV radiation, heat, or oxygen exposure (**Azwa *et al.*, 2013**). Besides that, the water that is taken up by the waste polypropylene can have an effect on this absorption band as water molecules show O-H stretching vibrations in this region (**Dai *et al.*, 2023**).
The asymmetric stretching vibrations of methyl ($–CH_3$) and methylene ($–CH_2$) groups in the polypropylene backbone are due to a peak at 2922.72 cm^{-1} (**Smith, 2021**). The peak at 2515.518 cm^{-1} is not typical for polypropylene that is standard and it may be due to impurities or additives. The peak at 1629.56 cm^{-1} might be given to (C=C) (**Vedula *et al.*, 2016**). The peak at 1460.76 cm^{-1} is related to ($–CH_3$) asymmetric deformation vibrations or ($–CH_2$) scissor vibrations (Morent et al., 2008) . In contrast,

the peaks at 844.40 cm^{-1} and 720.53 cm^{-1} are linked to methylene ($–CH_2$) rocking vibrations (**Li *et al.*, 2004**).

The FTIR spectrum of C-PP shows significant peaks which are the signals of different functional groups that were introduced during the pyrolysis process. The peak at 2855.56 cm^{-1} is definitely due to the symmetric stretching vibrations of methylene ($–CH_2$) groups (**Yao *et al.*, 2010**). The band at 1450 cm^{-1} can be assigned to the CH_2 bending vibrations, and the band at 720 cm^{-1} is related to the CH_2 rocking vibrations. These two motions of the CH_2 group are the main characteristic of the aliphatic hydrocarbon (**Zhang *et al.*, 2025**). The vibration at 1799.96 cm^{-1} can be tentatively assigned to the high-frequency C=O stretching of carbonyl groups **(Guo & Lin, 2014**). The presence of these groups defines the chemical transformations occurring during PP pyrolysis.

The FT-IR spectrum of Fe_3O_4 shows several characteristic peaks that match the vibrational modes of its molecular structure. The bands at 445.75 cm^{-1} and 600 cm^{-1} are due to Fe–O stretching vibrations of Fe_3O_4 (**Yuvakkumar & Hong, 2014**).The prominent peak at 3371 cm^{-1} indicates O–H stretching vibrations, suggesting the presence of adsorbed water or hydroxyl groups on the surface of Fe_3O_4 **(Chircov *et al.*, 2021**).

The FTIR spectrum of CQDs indicates the various functional groups that appear on their surface by different bands. The highest peak found at 3434.31 cm^{-1} is assigned to O–H stretching vibrations and it is indicative of the hydroxyl groups and surface hydration (**Chunduri *et al.*, 2016**). The peak at 2871.18 cm^{-1} is interpreted as a C–H stretching which means the presence of aliphatic hydrocarbons **(Janus *et al.*, 2019**). The signal at 1801.81 cm^{-1} refers to C=O stretching vibrations that are related to carbonyl or carboxyl groups which can be understood as the result of the oxidation process (**Mai *et al.*, 2020**). The band at 875.67 cm^{-1} is attributed to the out-of-plane bending of C–H in aromatic rings, confirming the presence of sp^2-hybridized carbon frameworks (**Papaioannou *et al.*, 2018**).

The FTIR spectrum of MCQDs reveals several peaks which are from the different functional groups that are on the material surface. The absorption band found at 3645.34 cm^{-1} corresponds to the stretching vibration of both free and hydrogen-bonded O H groups, which is the primary source of the hydroxyl functional groups or water molecules on the surface of the sensor (**Dai *et al.*, 2023**). The peak at 3434.31 cm^{-1} is due to O–H stretching vibrations of hydroxyl groups or water that is absorbed on the surface of the MCQDs. The band at 1398 cm^{-1} is due to the C–O stretching (**Alemu *et al.*, 2025**). The peak at 1050.30 cm^{-1} is due to the C–O stretching vibrations, which are the characteristic of oxygen containing functional groups that can possibly improve the stability and the dispersibility of MCQDs (**Das *et al.*, 2022**). The peak at 556.27 cm^{-1} is due to Fe-O vibrations and it is consistent with the presence of iron oxide nanoparticles in the MCQDs which are the source of their magnetism (**Mohapatra *et al.*, 2015**).

The functional groups of the MEG-MCQDs are represented in **Fig.3C**. The wide, high absorption band that was detected in the range of 3400–3500 cm^{-1} is attributed to the O-H stretching vibrations, thus it is a direct indication of hydroxyl groups that are introduced by monoethylene glycol functionalization **(Dai *et al.*, 2023; Eso *et al.*, 2025**). The peaks that appeared near 2920 cm^{-1} are C–H stretching vibrations, and they show the presence of aliphatic or alkyl chains on the surface of the carbon dots (**Rahardja *et al.*, 2025**). Besides, a peak around 1630 cm^{-1} is the C=O stretching vibration, a carboxyl or carbonyl group is the source of this peak

(**Ahluwalia, 2023; Moorthi *et al.*, 2025**). The intense bands located at the region 1000–1300 cm^{-1} are due to C–O stretching vibrations of alcohols and ethers, which are the same as the bands of the successful attachment of monoethylene glycol onto the carbon quantum dot structure (**Smith, 2022; Aka *et al.*, 2025**).

Table 2. Surface properties of Fe_3O_4, CQDS, MCQDs and MEG-MCQDS composites

Synthesized materials	**S_{BET} ($m^2.g^{-1}$)**	**V_P ($cc.g^{-1}$)**	**Pr (nm)**
Fe_3O_4	90	0.12	5.2
CQDS	360	0.2	2.7
MCQDS	245	0.5	3.3
MEG-MCQDS	280	0.35	2.7

2.Morphology of Fe_3O_4, CQDS, MCQDs and MEG-MCQDS composites

The SEM image of polypropylene waste (PP waste) illustrates a rough and fractured surface morphology at the microscale (**Fig.4a**). The material consists of irregular flakes and angular fragments, with sizes typically ranging from ~1 μm up to several micrometers, as indicated by the scale bar. The layered and cracked features are characteristic of polymer degradation and mechanical fragmentation. The OMEA treatment appears to further modify the surface, increasing roughness and creating additional fracture lines, which is consistent with chemical and structural alterations of the polymer surface.

The SEM image of carbon retrieved from waste polypropylene (C-PP) shows irregular, angular, and fragmented particles (**Fig. 4b**). The particle sizes range from ~500 nm to several micrometers, as observed from the scale bar. Surfaces appear mostly rough and uneven, consistent with the carbonaceous texture generated by pyrolysis. The non-uniform morphology reflects thermal decomposition effects during PP carbonization, leading to both compact fragments and finer debris.

The SEM image of Fe_3O_4 particles **(Fig. 4c)** shows angular, crystalline particles with sizes ranging from 50–100 nm, typical of magnetite. The morphology is primarily irregular and faceted, with some particles exhibiting elongated and fragmented structures.

The SEM image of CQDs (**Fig. 4d**) shows agglomerated nanoparticles with irregular, non-uniform morphology. The primary particles are estimated to be <20 nm, but they tend to form larger clusters in the submicron to micron range due to interparticle attractions such as Van der Waals forces. The surface texture appears rough and grainy.

The SEM image of MCQDs (**Fig. 4e**) reveals irregularly shaped nanoparticles aggregated into larger clusters. The particles display rough surfaces and angular morphology, consistent with Fe_3O_4 deposition on CQDs. While primary nanometric domains are present, the observed structures predominantly form aggregates ranging from several hundred nanometers to a few micrometers, as evident from the scale bar. The particle size histogram of MCQDs (**Fig.4h**) shows a dominant range of 300–400 nm, with sizes extending up to ~700 nm. This confirms that primary nanometric domains aggregate into submicron clusters, consistent with the SEM observations.

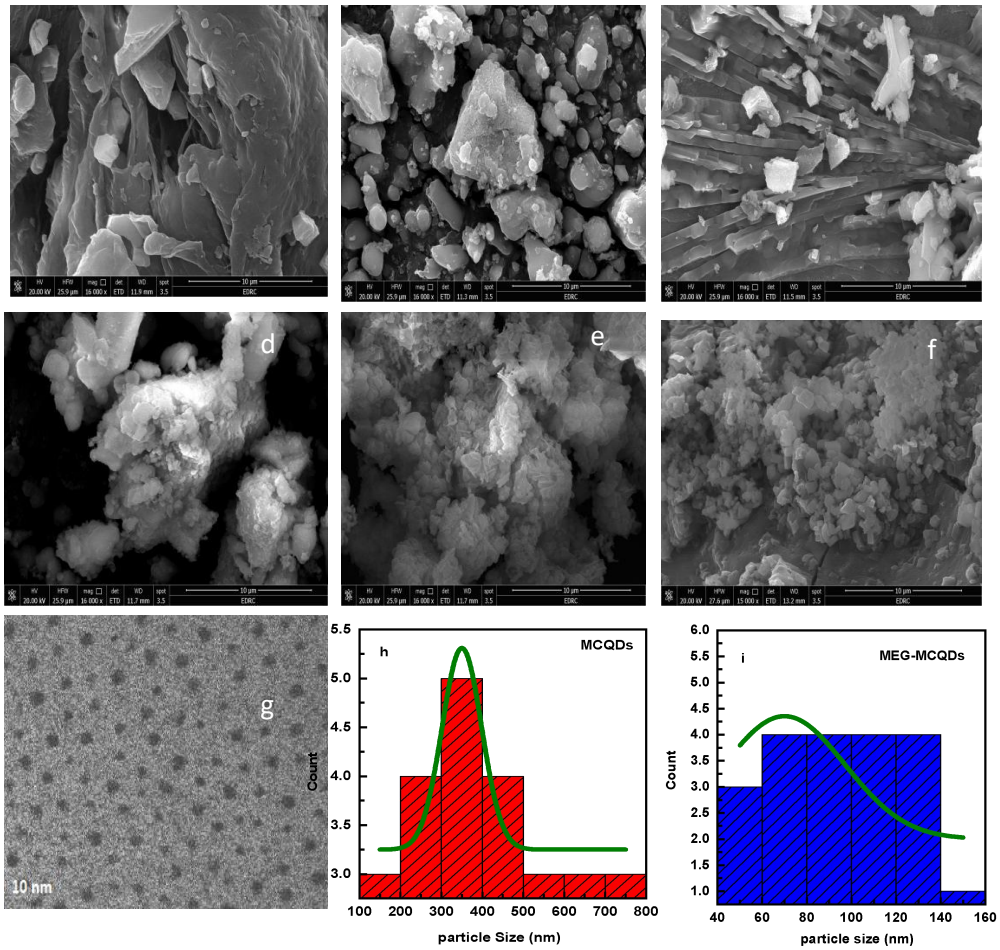

Fig.4. SEM of (a) PP waste, (b) C-PP, (c) Fe_3O_4, (d) CQDS, (e) MCQDs (f) and MEG-MCQDs composites, (g) TEM image of CQDS, and histogram of particle size distribution of h)MCQDs, and i) MEG-MCQDs.

The SEM image of MEG-MCQDs (**Fig. 4f**) reveals angular and block-like particles aggregated into large assemblies up to several micrometers. The histogram analysis (Fig.4i) further confirms that these assemblies are composed of primary particles in the 50–130 nm range, with an average size of ~70 nm. This indicates that MEG functionalization enhances crystallinity while promoting both nanoscale particle formation and their subsequent aggregation into micron-scale clusters.

The TEM image of CQDs (**Fig. 4g**) reveals well-dispersed nanoparticles with nearly spherical morphology. The average particle size is estimated to be in the 2–10 nm range, which falls within the expected size domain for carbon quantum dots. The uniform contrast indicates a relatively homogeneous size distribution, and no large agglomerates are observed under TEM, suggesting good dispersion stability compared to the SEM results.

3.Rheological Behavior

The rheological properties (PV, YP, and AV) remained stable across all concentrations of MEG-MCQDs and showed excellent thermal stability after hot rolling. This indicates that the nanomaterial can be added without negatively impacting the fluid's flow properties, which is crucial for predictable hydraulic performance during drilling (**Fig. 5a, b** and **Table 3**).

Plastic Viscosity (PV)

The results show that plastic viscosity (PV) (**Fig.5c** and **Table 3)** remains consistent across all mud formulations, both before and after hot rolling, with values ranging from 19 to 21 mPa•s. This suggests that the varying concentrations of water-based mud (WBM) additives do not significantly affect the mud's resistance to flow. The stable PV values indicate that the formulations maintain reliable flow behavior, even under thermal conditions, which is critical for performance in drilling operations. Also, the additives are most probably evenly distributed, which has prevented them from forming aggregates or clumps that might have changed the viscosity in an unexpected way.

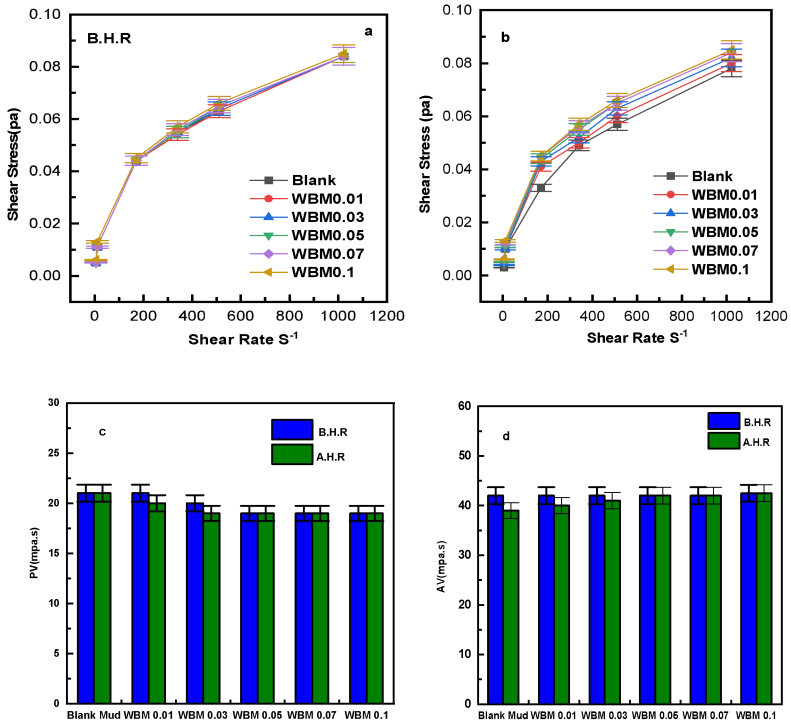

Fig.5.Shear rate and shear stress of drilling fluids with varying concentrations of MEG-MCQDs: (a) before hot rolling (BHR); (b) after hot rolling, c) Plastic Viscosity (PV) of drilling fluids BHR and AHR, d)Apparent Viscosity of drilling fluids BHR and AHR.

The minor reduction in PV after the hot rolling was more visible in the higher concentration WBM formulations and this indicates that the mud formulations have good thermal stability. It is the condition where the additives and the base fluid keep their characteristics at the higher temperatures thus allowing the flow performance to be reliable in the case of geothermal or deep-well drilling operations (**Abdelhafiz *et al.*, 2023; Majid, 2025**). The consistent PV over the different formulations shows that the mud's flow resistance is not going to be affected by the thermal stress, which is very important for the efficiency of pressure management, cooling, and cuttings transportation during the drilling process.

Apparent Viscosity (AV)

Apparent viscosity (AV) values (**Fig.5d**) and **Table 3** of Blank Mud and different water-based mud (WBM) formulations are within a narrow range of 39-42.5 mPa·s, and this trend remains unchanged after hot rolling. This suggests that the use of WBM additives does not lead to any considerable change in fluid's viscosity and the

formulations show a stable flow behavior under thermal treatment. The minimal rise in AV in the WBM0.01 and WBM0.03 mixtures after the hot rolling process might be explained by very small alterations of the mud structure, but the total effect is negligible. The mud formulations, in their entirety, are similar in their flow characteristics irrespective of the additive concentrations and or the treatment at high temperatures.

Gel Strength

The gel strength values (**Fig.6a**) and **Table 3** for Blank Mud and the WBM formulations vary within 3 to 6 lb/100ft², thus showing minor variations BHR and AHR. Blank Mud is still gel strength of 5 lb/100ft² in all the tests, while the WBM formulations are going up and down between 3 and 6 lb/100ft². The gels are produced on lower concentrations of WBM (0.01 and 0.03) which show a marginal decrease in gel strength after hot rolling that can be interpreted as a mud structure that is slightly weakened. The gel strength, however, is unchanged throughout which is an indication of good shear recovery as well as the capability of suspending cuttings **(Gao *et al.*, 2025; Mahmoud *et al.*, 2021**). The WBM0.1 formulation reflects a minor rise in gels strength after hot rolling, which is in all probability an aspect of the additive's thermal nature.

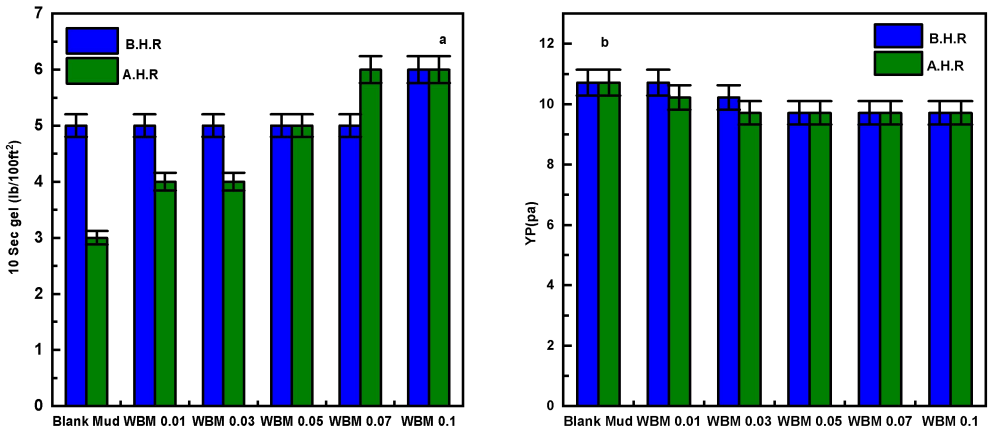

Fig.6. a) Gel strength of drilling fluids BHR and AHR, b) Yield point (YP) of drilling fluids BHR and AHR

Yield Point (YP)

The yield point (YP) values (Fig.6b) and Table 3 for Blank Mud and the water-based mud (WBM) formulations remain stable, ranging from 9.709 to 10.71 lb/100ft² before and after hot rolling (BHR and AHR). Blank Mud consistently shows a YP of 10.71 lb/100ft², while the WBM formulations experience a slight decrease after hot rolling, particularly in the WBM0.03 and higher concentrations, where the values drop to 9.709 lb/100ft². This implies that the mud's resistance to flow has slightly decreased due to thermal treatment, particularly in higher concentration formulations. Such a small decrease notwithstanding, the stability of YP throughout the formulations shows that the muds still have adequate flow properties to facilitate efficient hole cleaning and cuttings transport, even if the temperature is high during the drilling process **(Karakosta *et al.*, 2021; Mahmoud *et al.*, 2024; Oguta & Ihua-Maduenyi, 2025**).

Filtration and Cake Structure

The fluid loss (API FL) and filtrate loss data (**Fig.7a, b**) and **Table 3** for the Blank Mud and water-based mud (WBM) formulations exhibit characteristics that are almost identical during BHR and AHR. The API fluid loss numbers exhibit minimum variation of 6 mL for Blank Mud and all WBM formulations, in which WBM0.01 (8 mL) and WBM0.03 (7 mL) are slightly higher after hot rolling. According to the results, in general, the formulations show stable fluid loss characteristics, with small changes only, which might be due to the mud's microstructure changes caused by the elevated temperature. Nevertheless, the fluid loss is still at the acceptable level for most of drilling applications, which means that the mud is capable of sealing the wellbore and it will not lose too much fluid during the drilling operations **(Jiang *et al.*, 2022; Salem *et al.*)**.

The filter cake thickness data shows a similarly stable trend, with minimal variation across the formulations, ranging from 3.4 to 4 mm. While there is a slight increase in the filter cake thickness for most WBM formulations after hot rolling, the changes are small, indicating that the mud maintains an adequate filter cake formation even under thermal stress. This is important for ensuring that the mud can provide a reliable barrier between the drilling fluid and the formation, minimizing filtration losses.

.

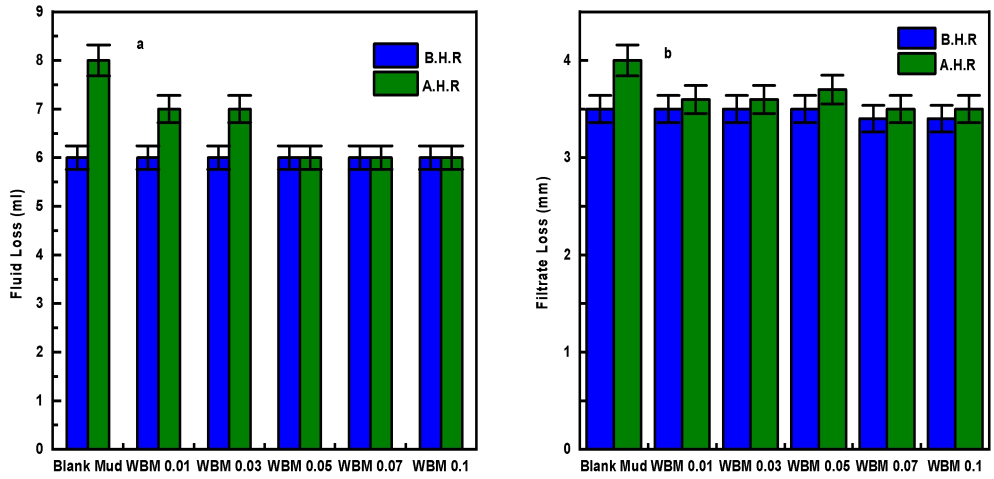

Fig.7 a) Fluid Loss (FL) of drilling fluids BHR and AHR and b)Filter Cake of drilling fluids BHR and AHR.

4.Lubricity Enhancement

Table 4 and Fig. 8 illustrate the effects of MEG-MCQDs nanoparticles on water-based mud (WBM) systems, with particular emphasis on water readings, mud readings, lubricity coefficient (LC), Correction factor (CF),Torque reduction and Friction Coefficient prior to and following hot rolling (BHR and AHR). The metrics offer insights into the performance of nanoparticle-treated muds under high-temperature conditions, which are essential for drilling operations.

Lubricity coefficient (LC)

The Lubricity Coefficient (LC) (**Table 4 and Fig. 8a)** measures the ability of drilling fluids to reduce friction between the drill string and wellbore, thereby enhancing drilling efficiency. In this dataset, Blank Mud shows the highest LC values, with 0.22 for BHR and 0.25 for AHR, indicating the poorest lubricity. Other formulations such as WBM0.01, WBM0.03, WBM0.05, WBM0.07, and WBM0.1

exhibit lower LC values, ranging from 0.134 to 0.158 for BHR and 0.136 to 0.158 for AHR, demonstrating improved lubricating properties compared to Blank Mud**.** Overall, MEG-MCQDs addition clearly enhances lubricity under both thermal conditions.

The variation in LC values over the various mud types is due to the different properties in each formulation of the mud. The Blank Mud formulation has the highest LC values, showing that it lacks efficient lubricating additives. By contrast, the WBM series (WBM0.01–WBM0.1) shows consistently lower LC values, confirming their effectiveness in lowering friction. The small increase in LC after hot rolling (AHR) suggests a minor thermal effect, but lubricity remains better than that of Blank Mud.

Table 3. Properties of Water-Based Geothermal Drilling Fluids with and Without Nanomaterial concentrations. Values are presented for rheological properties, (NA: Not Available).

	Blank Mud		**$WBM_{0.01}$**		**WBM0.03**		**$WBM_{0.05}$**		**WBM0.07**		**$WBM_{0.1}$**	
	BHR	**AHR**	**BHR**	**AHR**	**BHR**	**AHR**	**BHR**	**AHR**	**BHR**	**AHR**	**BHR**	**AHR**
R600	84	78	84	80	84	82	84	84	84	84	85	85
R300	63	57	63	60	64	63	65	65	65	65	66	66
R200	55	49	54	50	55	52	55	55	56	56	57	57
R100	44	33	44	41	44	43	44	44	44	45	45	45
R6	11	10	11	10	11	10	11	11	11	12	13	13
R3	5	3	5	4	5	4	5	5	5	6	6	6
R3'	7	5	7	5	7	6	7	7	7	7	8	7
	Blank Mud		**$WBM_{0.01}$**		**WBM0.03**		**$WBM_{0.05}$**		**WBM0.07**		**$WBM_{0.1}$**	
	BHR	**AHR**	**BHR**	**AHR**	**BHR**	**AHR**	**BHR**	**AHR**	**BHR**	**AHR**	**BHR**	**AHR**
YP (mPa.s)	10.71	10.71	10.71	10.22	10.22	9.709	9.709	9.709	9.709	9.709	9.709	9.709
PV (mPa.s)	21	21	21	20	20	19	19	19	19	19	19	19
AV	42	39	42	40	42	41	42	42	42	42	42.5	42.5
API FL (ml)	6	8	6	7	6	7	6	6	6	6	6	6
Filter Cake (mm)	3.5	4	3.5	3.6	3.5	3.6	3.5	3.7	3.4	3.5	3.4	3.5

Torque Reduction

The data characterizing the torque reduction (%) (**Table 4 and Fig. 8b)** of the different nanomaterial concentrations in water-based mud (WBM) illustrates a pronounced improvement trend in lubricity when the nanoparticle concentration was increased. According to this, the blank mud, which exhibits zero torque reduction, is the starting point. Next, the introduction of 0.01% nanomaterial leads to a torque reduction of 29.55% in BHR and 36.8% in AHR. As the concentration rises to 0.03%, 0.05%, and 0.07%, the torque reduction continues to increase and for the 0.07% concentration, it reaches 45.6% in AHR. When the highest concentration (0.1%) is reached, the torque reduction is at its maximum with 52.4% reduction in BHR and 46.82% in AHR. These findings are consistent with the LC results, where lower LC values correspond to higher torque reduction, confirming the beneficial effect of MEG-MCQDs on lubricity. These results indicate that the nanomaterial serves as the main factor behind the lubricating properties improvement of the drilling fluid that is most probably due to the formation of a protective boundary layer that decreases the

friction and the wear of the drill string(**Salem et al**.). The increase in torque reduction with the higher nanoparticle concentrations points out the promising role of these nanomaterials in supporting the energy-saving of geothermal drilling operations.

Friction Coefficient

The friction coefficients (**Table 4 and Fig. 8c)** of the various mud formulations, including the Blank Mud as well as WBM types, show the performance of the mud under frictional stress. The WBM formulations have a friction coefficient of 0.1005 for WBM0.01 (BHR) and 0.1780 for WBM0.1 (AHR). Lower friction coefficients correspond to better lubricity, consistent with the observed LC and torque reduction results. The numbers are consistent with a trend of increasing friction with the rise of additive concentration and after the thermal treatment (AHR), indicating that WBM additives at higher concentrations could be a source of friction ***(Singh et al.*, 2025**). This upward trend is indicative of the mud's lubricating properties being influenced by thermal treatment, hence, a minor reduction in its friction-reducing ability for higher additive concentrations. The WBM formulations clearly indicate the lubricating nature of the lower concentration formulations, however, the friction-reducing performance at high additive concentrations and heat treatment can be compromised.

Mechanism Interpretation of Lubricity for MEG-MCQDs Nanoparticle-Enhanced WBM Systems

The increase in lubricity of water-based geothermal drilling fluids (WBM) with MEG-functionalized MCQDs is mainly due to the creation of a protective boundary layer (**Lee *et al.*, 2025**). These nanoparticles are adsorbed on the metal surfaces of the drill string and wellbore, thus, a thin, protective film is formed that is a barrier to the direct contact of the metals (**Uwaezuoke, 2022;Gautam *et al.*, 2025**). This is not only reducing the friction and wear but also improving lubricity. The friction coefficient data shows a significant reduction in friction for the nanoparticle-treated muds compared to Blank Mud, both before and after exposure to high temperatures (BHR and AHR), supporting the role of the nanoparticles in reducing friction.

MEG-functionalized MCQDs are the main factors that help to keep the nanoparticles stably dispersed in the mud system and hence, they are able to carry out the uniform distribution effectively. This stabilization is further confirmed as it is reduction to the formation of particle agglomerates, which could be a negative impact to the lubricating property of the mud. Thus, through the well-dispersed nanostructure, these nanoparticles are the ones responsible for the decrease of the torque and friction coefficients in the drilling system. This is especially evident in the torque reduction values, which show improvement with higher concentrations of MEG-MCQDs, indicating better lubrication and energy efficiency in drilling operations.

In addition, the nano-spherical structure of the MCQDs also facilitates their motion due to the rotary effect in the liquid. These nanoparticles behave in the same way as nano ball bearings, thus giving the drill pipe and wellbore more lubrication, which leads to a decrease in sliding friction and a reduction of torque **(Chu *et al.*, 2023; Gokapai *et al.*, 2024; Wang *et al.*, 2025**). This kind of lubrication is very efficient because it reduces the need for energy, so the drilling can be done in a smooth way during the whole operation. Although friction coefficients increase slightly with higher additive concentrations and after thermal treatment, the overall lubricating effect remains stable, indicating that the nanoparticles continue to perform well under high-temperature conditions.

Moreover, the MEG-MCQDs's regenerating influence also plays an important role in friction reduction. The particles have the potential of repairing the micro-cracks and rough spots on surfaces of the metal, thus they are able to fill the roughness, smooth the asperities, and reduce the total friction. Such a smoothing effect on the surface is especially advantageous after the treatment with high temperature when it keeps the coefficient of lubricity (LC) stable, thus it guarantees that the best lubrication is provided throughout the whole drilling process. The lower torque values and the steady lubricating performance of the muds with nanoparticles support this statement.

The polishing effect is another important mechanism at play. Under high shear conditions, the nanoparticles continuously modify the surface interactions, maintaining smooth contact surfaces and reducing the adhesion between the drill string and the wellbore (**Wei *et al.*, 2024**). This is reflected in the consistently low friction coefficients observed across all concentrations of MEG-MCQDs, indicating that the particles effectively smooth and protect the surfaces, reducing the likelihood of wear and maintaining performance even after extended thermal exposure.

Table 4. **Parameters values, lubricity coefficient, and the percentage of torque reduction in blank and sample muds before and after hot rolling. (NA: Not Available). (Water reading=34)**

	Blank mud		**$WBM_{0.01}$**		**WBM0.03**		**$WBM_{0.05}$**		**WBM0.07**		**$WBM_{0.1}$**	
	BHR	**AHR**	**BHR**	**AHR**	**BHR**	**AHR**	**BHR**	**AHR**	**BHR**	**AHR**	**BHR**	**AHR**
Mud Reading	22	25	15.5	15.8	14.1	14.5	13.4	13.6	12.6	12.9	11.7	11.9
CF	1	1	1	1	1	1	1	1	1	1	1	1
LC	0.22	0.25	0.155	0.158	0.141	0.145	0.134	0.136	0.126	0.129	0.117	0.119
Torque Reduction (%)	NA	NA	29.55	36.8	35.91	42	39.09	45.6	42.73	48.4	46.82	52.4
Friction Coefficients	NA	NA	0.1005	0.1251	0.1222	0.1428	0.1329	0.1549	0.1450	0.1646	0.1592	0.1780

To further support this mechanism, we also considered the dispersion stability of the nanoparticles. Zeta potential values provide a useful indicator: Blank Mud typically shows low values around –10 to –15 mV, which explains its tendency to flocculate. When MCQDs are added, the values improve slightly (–20 to –25 mV), but some aggregation is still expected. In contrast, MEG-MCQDs exhibit highly negative values in the range of –35 to –40 mV, confirming that MEG functionalization increases electrostatic repulsion and helps keep the particles well dispersed in the mud. This stable dispersion makes it easier for the nanoparticles to spread evenly over the drill string and wellbore surfaces, forming protective boundary films and acting as nano-ball bearings. The friction coefficient results agree with this interpretation: lower values for the MEG-MCQD muds demonstrate that well-dispersed nanoparticles are directly responsible for the reduction in torque, friction, and wear under geothermal drilling conditions.

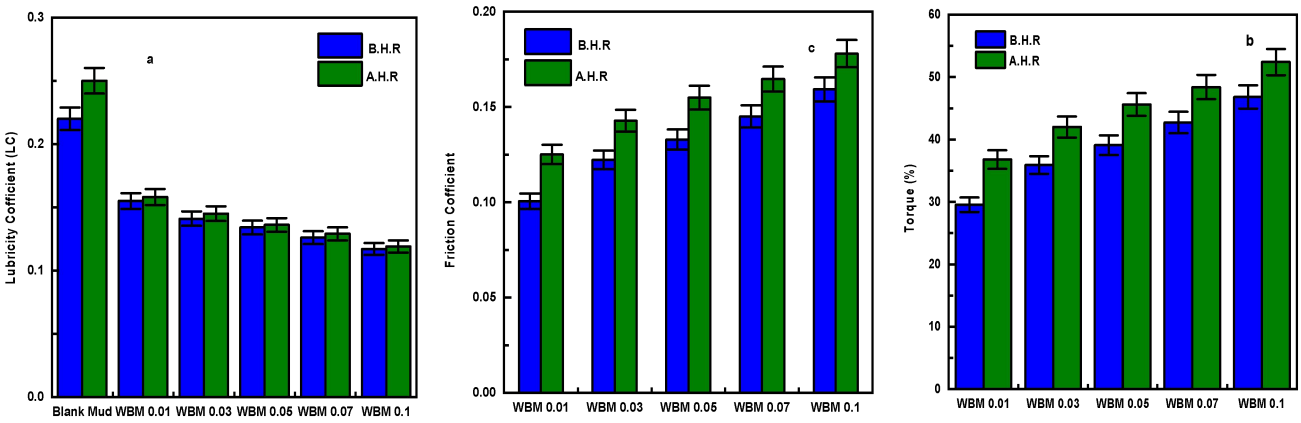

Fig.8.a) Lubricity Coefficient (LC), b) Torque Reduction (%) of geothermal drilling fluids before and after hot rolling. c) Friction Coefficient.

5.Comparison with Reported Nanomaterials

Benchmarking against literature shows that graphene, silica nanoparticles, and MWCNTs (Table 5)
provide friction or torque reductions ranging from 20% to 85% under various drilling conditions. In comparison,

MEG-MCQDs achieved up to 52.4% LC reduction with stable performance under both BHR and AHR conditions. This demonstrates that MEG-MCQDs offer competitive lubricity enhancement in the harsher environment of geothermal WBM, highlighting their novelty and practical value.

Table 5. Comparison of lubricity performance of different nanomaterials with MEG-MCQDs

Additive	Reported LC / COF Reduction	Conditions	Reference
Graphene	Up to 85% COF reduction (from 1.30 → 0.21); ~46–60% COF reduction in KCl brine muds	Water-based, brine systems	(**Zheng *et al.*, 2021**)
Silica (SiO_2) NPs	COF reduced from 0.37 → 0.11 (~70% reduction)	WBM at ~250 °F	(**Zhao *et al.*, 2022**)
MWCNTs	~20–36% torque / COF reduction	Oil-based emulsions, nanocapsule fluids	(**Lysakova *et al.*, 2024**)
MEG-MCQDs (This work)	Up to 52.4% LC reduction; stable under BHR and AHR conditions	Geothermal WBM	**This study**

Conclusion

This study demonstrates the potential of monoethylene glycol–based magnetic carbon quantum dots (MEG-MCQDs) as an effective additive for geothermal drilling fluids. At concentrations between 0.01% and 0.1% in water-based mud (WBM), MEG-MCQDs maintained stable rheological properties (PV, YP, and AV) and exhibited excellent thermal stability after hot rolling at 170 °C, indicating suitability for high-pressure, high-temperature (HPHT) conditions. Furthermore, the nanocomposite reduced torque by up to 52.4% at the maximum concentration,

highlighting its effectiveness in improving lubricity and reducing friction. Overall, the incorporation of MEG-MCQDs into drilling fluids offers a promising approach to enhancing drilling efficiency, protecting equipment, and supporting the sustainable development of geothermal energy.

Declarations:
Ethics Approval: Guidelines for this article were established by the Benha University's local ethics committee (ZD/FSc/BU-IACUC/2025).

Conflict of Interest: The authors declare no conflict of interest.

Author contribution: Anwaar O. Ali: Conceptualization, Methodology, Experimental Investigation, Writing – Original Draft, Writing – Review & Editing. Amany A. Aboulrous: Conceptualization, Methodology, Experimental Investigation, Validation, Project Administration, Writing – Review & Editing, Supervision. Mahmoud F. Mubarak: Validation, Writing – Review & Editing, Supervision. Mahmoud Ibrahim Abdou: Conceptualization, Methodology, Validation, Writing – Review & Editing, Supervision. A. M. Fadl: Writing – Review & Editing, Supervision. Wagdy I. El-Dougdoug: Writing – Review & Editing, Supervision. Aly A. Aly: Writing – Review & Editing, Supervision.

Data Availability Statement: Data is contained within the article.

Funding Information: The authors are gratful for the support from Centro para el Desarrollo Tecnológico Industrial (CDTI, Spain) and Science, Technology & Innovation Funding Authority (STDF, Egypt) under the grant ID (46666) titled "Nanofluids for geothermal drilling operations" within the framework of the: (Egyptian Spanish Joint Technological Co-operation Program) Grant.
Acknowledgment: We acknowledge the support and the help presented by Egyptian Petroleum Research Institute

REFERENCE

Abdelhafiz, M. M., Oppelt, J., Mahmoud, O., & Hegele, L. A. (2023). Effect of drilling and wellbore geometry parameters on wellbore temperature profile: Implications for geothermal production. *Advances in Geo-Energy Research*, *8*(3), 170-180.

Ahluwalia, V. (2023). Infrared spectroscopy. In *Instrumental Methods of Chemical Analysis* (pp. 179-231). Springer.

Ahmed, A., Pervaiz, E., Abdullah, U., & Noor, T. (2024). Optimization of Water Based Drilling Fluid Properties with the SiO2/g-C3N 4 Hybrid. *ACS omega*, *9*(13), 15052-15064.

Ahmed, A., Sharifi Haddad, A., Rafati, R., Bashir, A., AlSabagh, A. M., & Aboulrous, A. A. (2021). Developing a thermally stable ester-based drilling fluid for offshore drilling operations by using aluminum oxide nanorods. *Sustainability*, *13*(6), 3399.

Aka, B., Nwadiogbu, J., Oragwu, P., Igwe, D., Aka, S., Eberendu, K., & Nlemchukwu, B. (2025). ACETYLATION AND Characterization of African Star apple kernels (chrysophyllum albidum) for the preparation of crude oil sorption active material: physicochemical properties, ftir spectroscopy, and surface morphology analysis. *adsorption*, *62*(05).

Akhigbe, E. E. (2025). Advancing geothermal energy: A review of technological developments and environmental impacts. *Gulf Journal of Advance Business Research*.

Al Jaberi, J. B., Bageri, B., Adebayo, A. R., & Elkatatny, S. M. (2025). Enhancing Filter Cake Sealing in Ilmenite-Based Drilling Fluids Using Perlite: Performance Across Varied Densities and Filtration Media. *ACS omega*.

Al Shenabrah, H. T. H. (2021). *Using Continuous Circulation Technology to Improve Drilling Efficiency and Mitigate Downhole Problems* Politecnico di Torino].

Alemu, Y. A., Louw, C. J., Paolucci, F., Valenti, G., & Baker, P. G. (2025). Luminescence and Electroanalytical Properties of Carbon Quantum Dots in the Context of Immunosensor Design. *ChemElectroChem*, *12*(6), e202400624.

Ali, A. O., Morshedy, A. S., El-Zahhar, A. A., Alghamdi, M. M., & El Naggar, A. M. (2024). African continent: Rich land of minerals and energy sources. *Inorganic Chemistry Communications*, *169*, 113123.

Ali, I., Ahmad, M., Arain, A. H., Atashbari, V., & Zamir, A. (2022). Utilization of biopolymers in water based drilling muds. In *Drilling Engineering and Technology-Recent Advances New Perspectives and Applications*. IntechOpen.

Almubarak, T., AlKhaldi, M., Ng, J. H., & Nasr-El-Din, H. A. (2021). Matrix acidizing: A laboratory and field investigation of sludge formation and removal of oil-based drilling mud filter cake. *SPE Drilling & Completion*, *36*(02), 281-299.

Atta, M. R., Lal, B., Abdulwahab, A., Manjusha, A., Shariff, A. M., & Foo, K. S. (2025). Regenerated Monoethylene Glycol: A comprehensive systematic review of contaminant profiles and hydrate inhibition efficacy. *Journal of Industrial and Engineering Chemistry*, *147*, 1-19.

Azwa, Z., Yousif, B., Manalo, A., & Karunasena, W. (2013). A review on the degradability of polymeric composites based on natural fibres. *Materials & Design*, *47*, 424-442.

Bardhan, A., Singh, A., Nishanta, H., Sharma, S., Choubey, A. K., & Kumar, S. (2024). Biogenic copper oxide nanoparticles for improved lubricity and filtration control in water-based drilling mud. *Energy & Fuels*, *38*(10), 8564-8578.

Bassetti, J., Poulesquen, A., & Pierlot, C. (2024). Review on Cutting Fluids: Formulation, Chemistry and Deformulation. *Journal of oleo science*, *73*(7), 921-941.

Cao, M., Li, Y., Song, X., Chen, Y., Sun, L., Shi, X., Dai, C., & Yuan, B. (2023). Carbon dots nanofluid: Reducing injection pressure in unconventional reservoir by regulating oil/water/rock interfacial properties. *Fuel*, *352*, 129046.

Capuano Jr, L. E. (2025). Geothermal well drilling. In *Geothermal Power Generation* (pp. 125-158). Elsevier.

Chenic, A. Ș., Cretu, A. I., Burlacu, A., Moroianu, N., Vîrjan, D., Huru, D., Stanef-Puica, M. R., & Enachescu, V. (2022). Logical analysis on the strategy for a sustainable transition of the world to green energy—2050. Smart cities and villages coupled to renewable energy sources with low carbon footprint. *Sustainability*, *14*(14), 8622.

Chircov, C., Matei, M.-F., Neacșu, I. A., Vasile, B. S., Oprea, O.-C., Croitoru, A.-M., Trușcă, R.-D., Andronescu, E., Sorescu, I., & Bărbuceanu, F. (2021). Iron oxide–silica core–shell nanoparticles functionalized with essential oils for antimicrobial therapies. *Antibiotics*, *10*(9), 1138.

Chu, A., Li, C., Zhou, Z., Liu, B., Zhang, Y., Yang, M., Gao, T., Liu, M., Zhang, N., & Dambatta, Y. S. (2023). Nanofluids minimal quantity lubrication machining: from mechanisms to application. *Lubricants*, *11*(10), 422.

Chunduri, L., Kurdekar, A., Patnaik, S., Dev, B. V., Rattan, T. M., & Kamisetti, V. (2016). Carbon quantum dots from coconut husk: evaluation for antioxidant and cytotoxic activity. *Materials Focus*, *5*(1), 55-61.

Dai, F., Zhuang, Q., Huang, G., Deng, H., & Zhang, X. (2023). Infrared spectrum characteristics and quantification of OH groups in coal. *ACS omega*, *8*(19), 17064-17076.

Das, A., Kundelev, E. V., Vedernikova, A. A., Cherevkov, S. A., Danilov, D. V., Koroleva, A. V., Zhizhin, E. V., Tsypkin, A. N., Litvin, A. P., & Baranov, A. V. (2022). Revealing the nature of optical activity in carbon dots produced from different chiral precursor molecules. *Light: Science & Applications*, *11*(1), 92.

Du, C., Chang, Z., Yu, H., Zhu, Y., Ma, Y., Ma, G., Yan, Y., Wang, C., Wang, W., & Cheng, Y. (2022). Magnetic quantum dots-stabilized foam fluid for enhanced oil recovery. *Chemical Engineering Journal*, *450*, 138334.

Duran, B. (2024). *Influence of gear transmission oils degradation on tribological performance and gearbox efficiency* INSA Lyon].

Elugoke, S. E., Uwaya, G. E., Quadri, T. W., & Ebenso, E. E. (2024). Carbon quantum dots: basics, properties, and fundamentals. In *Carbon dots: recent developments and future perspectives* (pp. 3-42). ACS Publications.

Eso, R., Tufaila, T., & Arman, A. (2025). Using FTIR Analysis to Investigate the Mineralogical Composition of Ultisolsa Alfisol in Southeast East Sulawesi, Indonesia. *INDONESIAN JOURNAL OF APPLIED PHYSICS*, *15*(1), 84-97.

Eze, V. H. U., Eze, E. C., Alaneme, G. U., & Bubu, P. E. (2025). Recent progress and emerging technologies in geothermal energy utilization for sustainable building heating and cooling: a focus on smart system integration and enhanced efficiency solutions. *Frontiers in Built Environment*, *11*, 1594355.

Fan, W., Zhuang, G., Li, Q., Yuan, P., & Liu, D. (2025). Review of Nanoparticles in Water-Based Drilling Fluids: Innovations, Challenges, and Future Directions. *Energy & Fuels*, *39*(19), 8800-8826.

Gao, F., Xu, P., Zhang, H., Wang, H., Zhao, X., Li, X., & Zhang, J. (2025). Preparation of a Nanomaterial–Polymer Dynamic Cross-Linked Gel Composite and Its Application in Drilling Fluids. *Gels*, *11*(8), 614.

Gautam, R., Sahai, M., & Kumar, S. (2025). Recent advances in application of nanomaterials as additives for drilling fluids. *Energy Sources, Part A: Recovery, Utilization, and Environmental Effects*, *47*(1), 3496-3519.

Ghasemi, K., Akbari, A., Jahani, S., & Kazemzadeh, Y. (2025). A critical review of life cycle assessment and environmental impact of the well drilling process. *The Canadian Journal of Chemical Engineering*, *103*(6), 2499-2526.

Gokapai, V., Pothana, P., & Ling, K. (2024). Nanoparticles in drilling fluids: a review of types, mechanisms, applications, and future prospects. *Eng*, *5*(4), 2462-2495.

Guo, Z., & Lin, Q. (2014). Coupling reaction of CO2 and propylene oxide catalyzed by DMC with co-complexing agents incorporated via ball milling. *Journal of Molecular Catalysis A: Chemical*, *390*, 63-68.

Holder, C. F., & Schaak, R. E. (2019). Tutorial on powder X-ray diffraction for characterizing nanoscale materials. In (Vol. 13, pp. 7359-7365): ACS Publications.

Igwe, C. I. (2021). Geothermal energy: a review. *Int. J. Eng. Res. Technol.(IJERT)*, *10*, 655-661.

Ikram, R., Mohamed Jan, B., Sidek, A., & Kenanakis, G. (2021). Utilization of eco-friendly waste generated nanomaterials in water-based drilling fluids; state of the art review. *Materials*, *14*(15), 4171.

Janus, Ł., Piątkowski, M., Radwan-Pragłowska, J., Bogdał, D., & Matysek, D. (2019). Chitosan-based carbon quantum dots for biomedical applications: synthesis and characterization. *Nanomaterials*, *9*(2), 274.

Jaya, M. F. P. (2025). Experimental Study on Eco-Friendly Additives for Improving Water-Based Drilling Fluid Stability at High Temperature Application.

Jiang, G., Sun, J., He, Y., Cui, K., Dong, T., Yang, L., Yang, X., & Wang, X. (2022). Novel water-based drilling and completion fluid technology to improve wellbore quality during drilling and protect unconventional reservoirs. *Engineering*, *18*, 129-142.

Kalhor Mohammadi, M., Riahi, S., & Boek, E. S. (2023). An insight review on formation damage induced by drilling fluids. *Reviews in Chemical Engineering*, *39*(3), 387-415.

Karakosta, K., Mitropoulos, A. C., & Kyzas, G. Z. (2021). A review in nanopolymers for drilling fluids applications. *Journal of Molecular Structure*, *1227*, 129702.

Khandaker, A. A. B., Ahmed, N., & Alam, M. S. (2023). Rheology and lubricity characteristics study at different temperatures using synthesized SnO2 nanoparticles in KCl free bentonite water base mud. *Petroleum Research*, *8*(4), 541-549.

Lee, S., Farfan-Cabrera, L., Iglesias, P., & Erdemir, A. (2025). Lubricating ability of a protic ionic liquid as an additive to an ultra-low viscosity synthetic oil under electrified sliding conditions. *Wear*, *570*, 205935.

Li, H.-W., Strauss, H. L., & Snyder, R. G. (2004). Differences in the IR methylene rocking bands between the crystalline fatty acids and n-alkanes: Frequencies, intensities, and correlation splitting. *The Journal of Physical Chemistry A*, *108*(32), 6629-6642.

Lysakova, E., Skorobogatova, A., Neverov, A., Pryazhnikov, M., Rudyak, V. Y., & Minakov, A. (2024). A comprehensive study of the effect of multi-walled carbon nanotubes as an additive on the properties of oil-based drilling fluids. *Journal of Materials Science*, *59*(11), 4513-4532.

Mahmoud, H., Alhajabdalla, M., Nasser, M. S., Hussein, I. A., Ahmed, R., & Karami, H. (2021). Settling behavior of fine cuttings in fiber-containing polyanionic fluids for drilling and hole cleaning application. *Journal of Petroleum Science and Engineering*, *199*, 108337.

Mahmoud, H., Mohammed, A. A., Nasser, M. S., Hussein, I. A., & El-Naas, M. H. (2024). Green drilling fluid additives for a sustainable hole-cleaning performance: a comprehensive review. *Emergent Materials*, *7*(2), 387-402.

Mai, X.-D., Phan, Y. T. H., & Nguyen, V.-Q. (2020). Excitation-Independent Emission of Carbon Quantum Dot Solids. *Advances in Materials Science and Engineering*, *2020*(1), 9643168.

Majid, T. M. (2025). *The effect of changing the density of oil well drilling fluid on the speed and efficiency of drilling* Ministry of Higher Education].

Martin, C., Babaie, M., Nourian, A., & Nasr, G. (2023). Designing Smart drilling fluids using modified nano silica to improve drilling operations in Geothermal wells. *Geothermics*, *107*, 102600.

Mashkoor, H. H., Ruhaif, D., Faisal, M., & Majed, A. K. H.(2025). A Project Adding Nanomaterials to Drilling Fluids.

Medina, O. E., Rosales, S., Garzón, N., López, D., Taborda, E. A., Ordonez, J. C., Fernandez, S. A., Cortés, F. B., & Franco, C. A. (2024). Advances in quantum dot applications for the oil and gas industry: current trends and future directions. *Energy & Fuels*, *38*(22), 21793-21831.

Meng, B., Yan, G., He, P., Zhou, Q., Xu, W., & Qiao, Y. (2025). Nanotechnology applications in geothermal energy systems: Advances, challenges and opportunities. *Advances in Geo-Energy Research*, *15*(2), 172-180.

Mohapatra, J., Mitra, A., Tyagi, H., Bahadur, D., & Aslam, M. (2015). Iron oxide nanorods as high-performance magnetic resonance imaging contrast agents. *Nanoscale*, *7*(20), 9174-9184.

Moorthi, P. V., Bavyataa, V., Vignesh, K., Divya Sri, K., & Balasubramani, R. (2025). Carbon Nanomaterials in Plant Nanotechnology. In *Plant Nanotechnology Fundamentals and Methodologies* (pp. 241-258). Springer.

Morales, R. (2025). Innovative Multifunctional Chemistry to Remove Oil Based Mud Filter Cake and Remediate Near Wellbore Damage Producing Wells After Well Communication. SPE International Conference on Oilfield Chemistry,

Morent, R., De Geyter, N., Leys, C., Gengembre, L., & Payen, E. (2008). Comparison between XPS-and FTIR-analysis of plasma-treated polypropylene film surfaces. *Surface and Interface Analysis: An International Journal devoted to the development and application of techniques for the analysis of surfaces, interfaces and thin films*, *40*(3-4), 597-600.

Oguta, E., & Ihua-Maduenyi, I. E. (2025). Performance Evaluation of Mucuna Solannie as a Sustainable Additive in Water-Based Drilling Mud Formulation: A Review. *Performance Evaluation*, *9*(5), 66-81.

Papaioannou, N., Marinovic, A., Yoshizawa, N., Goode, A. E., Fay, M., Khlobystov, A., Titirici, M.-M., & Sapelkin, A. (2018). Structure and solvents effects on the optical properties of sugar-derived carbon nanodots. *Scientific Reports*, *8*(1), 6559.

Rahardja, M. R., Kurniawan, D., Laysandra, T., & Chiang, W.-H. (2025). Graphene Quantum Dot–Cross-Linked Bioresource Hydrogels for Selective Molecular Capture in Therapeutic Loading and Environmental Remediation. *ACS Applied Nano Materials*.

Raza, M. A., Al-Khasawneh, M. A., Alharthi, Y. Z., Faheem, M., Haider, R., & Kumar, L. (2025). Power generation expansion planning with high penetration of geothermal energy–Potential, prospects and policy. *Environmental and Sustainability Indicators*, *26*, 100614.

Salem, H. M., Abbas, A. M., Sattar, A. A., Hassan, M. M., & Saad, A. L. A. R. Optimization of drilling parameters for efficient wellbore stability: A literature reviews.

Sani, S., Adnan, R., Oh, W.-D., & Iqbal, A. (2021). Comparison of the surface properties of hydrothermally synthesised Fe3O4@ C nanocomposites at variable reaction times. *Nanomaterials*, *11*(10), 2742.

Shah, M., Prajapati, M., & Pardiwala, J. M. (2025). Nanotechnology origination: a development path for petroleum upstream industry. *Chemical Papers*, 1-15.

Singh, A., Bardhan, A., Yadav, S., Sharma, S., & Choubey, A. K. (2025). Application of Phyto-Mediated Microwave-Synthesized ZnO-SnO2 Nanocomposites in Water-Based Drilling Fluids. *Industrial & Engineering Chemistry Research*.

Smith, B. (2021). The infrared spectra of polymers III: Hydrocarbon polymers.

Smith, B. (2022). The infrared spectra of polymers, VI: Polymers with CO bonds.

Srivastava, V., Beg, M., Sharma, S., & Choubey, A. K. (2021). Application of manganese oxide nanoparticles synthesized via green route for improved performance of water-based drilling fluids. *Applied Nanoscience*, *11*(8), 2247-2260.

Uwaezuoke, N. (2022). Polymeric nanoparticles in drilling fluid technology. In *Drilling Engineering and Technology-Recent Advances New Perspectives and Applications*. IntechOpen.

Vedula, V. B., Chopra, M., Joseph, E., & Mazumder, S. (2016). Preparation and characterization of nanoparticles of carboxymethyl cellulose acetate butyrate containing acyclovir. *Applied Nanoscience*, *6*(2), 197-208.

Wang, L., Wang, F., Niu, L., Li, X., Wang, Z., & Yan, S. (2025). Study on generation characteristics of a triboelectric ball bearing with defects. *Industrial Lubrication and Tribology*, *77*(3), 341-348.

Wei, J., Liu, W., Gao, D., & Guo, D. (2024). Effect of Polishing on Cutting Efficiency and Mechanical Properties of PDC Cutters. *SPE Journal*, *29*(02), 700-713.

Yalshetti, S., Thokchom, B., Bhavi, S. M., Singh, S. R., Patil, S. R., Harini, B., Sillanpää, M., Manjunatha, J., Srinath, B., & Yarajarla, R. B. (2024). Microwave-assisted synthesis, characterization and in vitro biomedical applications of Hibiscus rosa-sinensis Linn.-mediated carbon quantum dots. *Scientific Reports*, *14*(1), 9915.

Yang, X., Jiang, G., Liu, F., He, Y., Liu, R., & Dong, T. (2023). Lubricity and mechanism of catechol-based biomimetic lubricant in water-based drilling fluid. *Tribology International*, *188*, 108862.

Yao, X., Peng, Y., Zhou, Q., Xiao, P., & Sun, S. (2010). Distinction of eight Lycium species by Fourier-transform infrared spectroscopy and two-dimensional correlation IR spectroscopy. *Journal of Molecular Structure*, *974*(1-3), 161-164.

Yuvakkumar, R., & Hong, S. I. (2014). Green synthesis of spinel magnetite iron oxide nanoparticles. *Advanced Materials Research*, *1051*, 39-42.

Zhang, L., Zhao, H., Zhang, L., Song, R., Wang, Q., & Liu, Z. (2025). Effect of coal tar components and thermal polycondensation conditions on the formation of mesophase pitch. *Materials*, *18*(5), 1002.

Zhang, Q., Li, S., Zhang, W., & Peng, K. (2021). Influence of processed parameters on the magnetic properties of Fe/Fe3O4 composite cores. *Journal of Materials Science: Materials in Electronics*, *32*(1), 1233-1241.

Zhao, X., Li, D., Zhu, H., Ma, J., & An, Y. (2022). Advanced developments in environmentally friendly lubricants for water-based drilling fluid: a review. *RSC advances*, *12*(35), 22853-22868.

Zheng, Y., Asif, A., Amiri, A., & Polycarpou, A. A. (2021). Graphene-based aqueous drilling muds as efficient, durable, and environmentally friendly alternatives for oil-based muds. *ACS Applied Nano Materials*, *4*(2), 1243-1251.

Zhou, Y., Shan, Y., Xiao, L., Song, X., Bao, W., Ma, H., Li, H., Wu, X., & Wang, R. (2025). Modified Carbon Quantum Dots Based Nanocomposite System ?for Enhanced Oil Recovery in Low Permeability Reservoir. *Energy & Fuels*, *39*(9), 4204-4220.